Available online at www.sciencedirect.com
SCIENCE DIRECT®
Journal of the European Ceramic Society 26 (2006) 27–36
www.elsevier.com/locate/jeurceramsoc

Multilayer coatings with improved reliability produced by aqueous electrophoretic deposition

Begoña Ferrari*, Sergio González, Rodrigo Moreno, Carmen Baudín

Instituto de Cerámica y Vidrio, CSIC, Campus de Cantoblanco, E-28049 Madrid, Spain

Received 26 May 2004; received in revised form 19 October 2004; accepted 29 October 2004
Available online 30 December 2004

Abstract

Laminates in the system Al_2O_3/Y-TZP have been produced by an aqueous electrophoretic deposition (EPD) process combined with the use of thermogelling polysaccharides. Mixtures with relative volume ratios of Al_2O_3 to Y-TZP of 95/5, 60/40 and 0/100 have been studied in terms of colloidal stability, gelation behaviour and EPD kinetics. A graded symmetrical architecture, with external layers of A95Z5, and intermediate layers of A60Z40 sandwiching a layer of A0Z100 has been designed by controlling the sequential EPD kinetics of each suspension. The fracture strength of monoliths and laminates has been studied by three point bending and Weibull analysis. Even though the multilayer does not present strength values significantly higher than those of the A95Z5 monolith it presents enhanced reliability, as demonstrated by a higher Weibull modulus. Reliability of the laminate, under critical fracture conditions such as those involved in strength testing, is mostly due to a strong effect of the reduced thickness of the A95Z5 layers as compared to total thickness of the A95Z5 monolith.

Keywords: Films; Mechanical properties; Microstructure; Strength; Laminates; Al_2O_3/TZP; Electrophoretic deposition

1. Introduction

Electrophoretic deposition (EPD) is a reliable, low cost method for producing laminates thicker than those attainable with chemical deposition techniques, and is suitable for a wide range of compositions. Consequently, EPD is receiving increased attention for the fabrication of laminated and graded (step-graded or continuously graded) materials, either as self-supported materials or as coatings.

Several publications describe the experimental devices and parameters used to obtain laminated materials by EPD for either functional or structural applications.[1–21] Tables 1 and 2 review published papers dealing with fabrication of laminated and graded materials, respectively. In these tables, the formulation of the colloidal suspensions is shown, as well as the composition, geometry and dimensions of the resulting laminates.

Studies on EPD of laminated materials (Table 1) mostly focus on the determination of processing parameters involved in the preparation of alternating layers of Al_2O_3 and tetragonal ZrO_2, while those describing the fabrication of graded materials (Table 2) mainly deal with the improvements reached in structural properties such as toughness and hardness. The testing conditions and the mechanical properties determined on such layered structures are summarized in Table 3. In the most general case, characterization is performed in terms of Vickers indentation hardness and toughness and very little attention has been paid to bulk properties that would be strongly determined by the processing method, such as strength.

In a previous work,[22] the Weibull distribution of strength values, determined by three point bending with 20 mm span and a cross head rate of 0.5 mm/min, for thin (≈170 μm) 10 mm × 25 mm plates made on alumina with 5 vol.% of tetragonal zirconia (A95Z5) was found to be well described by a simple two parameter Weibull distribution, giving an average strength of ≈160 MPa, and a Weibull modulus around 3. In agreement with the low Weibull modulus, indicating

* Corresponding author.
E-mail address: bferrari@icv.csic.es (B. Ferrari).

0955-2219/$ – see front matter © 2004 Elsevier Ltd. All rights reserved.
doi:10.1016/j.jeurceramsoc.2004.10.018

Table 1
Laminated materials obtained by EPD

Reference	Laminated materials	Colloidal suspension formulation		Final material characteristics		
		Media	Additives	Geometry	Laminated thickness	Layers thickness (μm)
Sarkar et al.[1]	Al_2O_3/Y-TZP	Ethanol	HCl (pH < 5)	Planar	1.5 mm (80 layers)	2–1
Sarkar et al.[2]	Al_2O_3/Y-TZP	Ethanol	HCl (pH < 5)	Radial	350 μm (36 layers)	
Bissinger et al.[3]	ZTA/Y-TZP/Laz	Ethanol	HCl (pH < 5)	Planar	2.5 mm (>100 layers)	2–30
Sarkar et al.[4]	Y-TZP/Al_2O_3	Ethanol	HCl (pH < 5)	Planar		13–21
Fisher et al.[5]	Al_2O_3/Y-TZP	H_2O		Planar		8–20
Vandeperre et al.[6]	SiC/C	*n*-Butylamine + 5% acetone + 20% isopropanol		Radial		10–100
Ferrari et al.[7]	Al_2O_3/Y-TZP	H_2O	Dolapix CE64	Planar	10 layers	25–50
Zhitomirsky and Gal-Or[8]	Al_2O_3/Ce-TZP	Isopropanol		Radial	20 layers	1–10

Table 2
Graded materials obtained by EPD

Reference	Graded materials	Colloidal suspension		Material characteristics		
		Media	Additives	Geometry	Laminated thickness	Layers thickness
Sarkar et al.[9]	Al_2O_3/Y-TZP	Ethanol	Acetic acid	Planar	6 mm	
Ding et al.[10]	Ni/Al_2O_3 Cu/Al_2O_3	Ni^{2+} aqueous solution Cu^{2+} aqueous solution				
Merk[11]	Ni/SiC	Ni^{2+} aqueous solution				
Barmak et al.[12]	Al_2O_3/Al/Ni	Ni^{2+} aqueous solution		Planar	110 μm	20–40 μm
Sarkar et al.[13]	Al_2O_3/Ni Y-TZP/Ni Al_2O_3/$MoSi_2$	Ethanol	pH < 5	Planar		
Zhao et al.[14]	Y-TZP/Ce-TZP	*n*-Butylamine	PVA	Planar	1.8 mm	
Zhao et al.[15]	Al_2O_3/Ce-TZP	*n*-Butylamine + acetone	PVA	Radial	3 mm	
Börner and Herbig[16]	58AZ/48AZ	H_2O	Dolapix PC21	Planar	2.3 mm	
Put et al.[17]	WC–6% Co/WC–25% Co	*n*-Butylamine + acetone		Planar	2.3 mm	
Put et al.[18]	Y-TZP/WC	*n*-Butylamine + acetone		Planar	2 mm	
Vleugels et al.[19]	Al_2O_3/Y-TZP/Al_2O_3	*n*-Butylamine + acetone		Planar	5 mm	
Kaya[20]	Al_2O_3/Y-TZP	H_2O	Celor	Radial		Nanostructure

Table 3
Properties of laminates produced by EPD

References	Materials	Thickness	Mechanical test conditions	Mechanical properties
Vanderperre et al.[6]	SiC/C	1–2 mm (125 cm^2)	3 points bending, 0.05 mm/s charge rate, 20 mm span	Crack deflection
Prakash et al.[2]	Al_2O_3/Y-TZP	–	Microindentation Vickers (8 kgf load)	Crack deflection
			4 points bending	95% Y-TZP: 995 MPa, 75 kJ/m^2; 95% Al_2O_3: 488 MPa, 17.8 kJ/m^2
Sarkar et al.[9]	Al_2O_3/Y-TZP	6 mm	Vickers microindentation (3 kgf load)	$H_V = 26 - 15$ GPa; $K_{IC} = 2.5$–10 MPa $m^{1/2}$
Ding et al.[10]	Ni/Al_2O_3, Cu/Al_2O_3	–	Vickers microindentation (0.05 kgf load)	H_V, increases with a Ni matrix
			Pin-on-disc	Increases wear and adhesion
Zhao et al.[14]	Y-TZP/Ce-TZP	2.1 mm (9 cm^2)	Vickers microindentation (5 kgf load)	$H_V = 12.6 - 10.3$ GPa; $K_{IC} = 3.4$–10.2 MPa $m^{1/2}$
Zhao et al.[15]	Al_2O_3/Ce-TZP	1 mm (tubular)	Vickers microindentation (5 kgf load)	$H_V = 14.5 - 10.5$ GPa; $K_{IC} = 2$–10.2 MPa $m^{1/2}$
Put et al.[17]	WC–6% Co/WC–25% Co	1.5 mm (9 cm^2)	Vickers microindentation (0.5 and 10 kgf load)	$H_{V0.5} = 21 - 9$ GPa; $H_{V10} = 19 - 8.5$ GPa
Vleugels et al.[19]	Al_2O_3/Y-TZP/Al_2O_3	5 mm	X-ray diffraction, residual stresses	$\sigma(Al_2O_3) = 92 \pm 5$ MPa
Kaya et al.[20]	Al_2O_3/Y-TZP		Vickers microindentation	$H_V = 19.4$–10.4 GPa; $K_{IC} = 3.1$–7.1 MPa $m^{1/2}$

a broad range of strength values, fractographic observations demonstrated that fracture originated by cracks formed in the processing-related surface irregularities that grow intergranularly.

Multilayer coatings have received great attention to improve the mechanical behaviour of coatings. Depending on the constituents, reduction of the defect size due to the presence of interfaces between the layers, blunting of the crack tip by plastic deformation and/or deflection of the crack path near the interfaces have been identified as possible crack inhibiting mechanisms in multilayer coatings.[23,24]

In this work, a modification of the thin monolithic plates of alumina + 5 vol.% of tetragonal zirconia (A95Z5) is studied to assure hardness of the laminate, provided by external layers of the same composition (95A5Z), and enhanced mechanical behaviour. A graded symmetrical internal architecture, with two layers of 60 vol.% of alumina and 40 vol.% of tetragonal zirconia (A60Z40) sandwiching a layer made of tetragonal zirconia (A0Z100), has been designed to improve the mechanical behaviour of the coating compared to that of monolithic thin plates of the same composition as that of the constituent layers. The colloidal process of Gel-Electrophoresis was used to design and obtain the studied materials.[25]

2. Experimental

Stabilized aqueous suspensions of mixtures of alumina (Al_2O_3, Condea HPA05, USA) and tetragonal zirconia polycrystalline powder with 3 mol% Y_2O_3 (Y-TZP, TZ3YS, TOSOH, Japan) were prepared in deionized H_2O with the following powder compositions: 95 vol.% Al_2O_3/5 vol.% Y-TZP (A95Z5), 60 vol.% Al_2O_3/40 vol.% Y-TZP (A60Z40) and 100 vol.% Y-TZP (A0Z100). Al_2O_3 powders have a mean particle size of 0.35 μm and a specific surface area of 9.5 m^2/g, and Y-TZP powders have a mean particle size of 0.4 μm and a surface area of 6.7 m^2/g. Al_2O_3 /Y-TZP suspensions (A/Y-TZP) were prepared to final solids content of 14 vol.%, and stabilized adding 0.3 wt.% of a commercial polyelectrolyte (Dolapix CE64, Zschimmer-Schwarz, Germany), assuring that both powders, Al_2O_3 and Y-TZP, have a similar zeta potential (−30 mV).[7] Suspensions were ultrasonically homogenized using a 400 W sonication probe (IKA U400S, Germany) for 2 min.

A commercial carrageenan powder (Secogel TC, Hispanagar, Spain) was used as gelling agent. A 2 wt.% solution of carrageenan was prepared by heating at 90 °C up to dissolution and maintained at 60–65 °C. Suspensions were heated at 60–65 °C and mixed with the amount of carrageenan solution to reach a final concentration of 0.6 wt.% with regard to the water content.

The thermogelling behaviour of each suspension was determined by measuring the evolution of the viscosity versus temperature using a Rheometer RS50 (Haake, Germany). The sensor system consisted of a double-cone rotor and a stationary plate, protected with a solvent trap to reduce evaporation. Similar studies were carried out for all prepared suspensions.

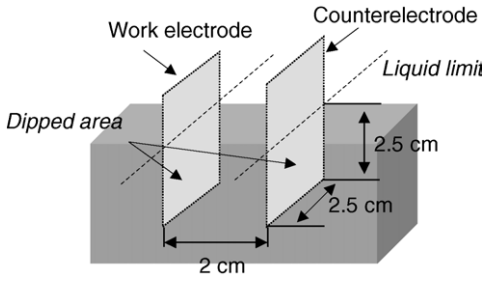

Fig. 1. Scheme of the EPD device.

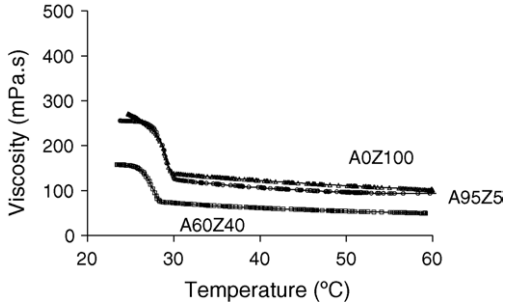

Fig. 2. Evolution of viscosity on cooling of A95Z5, A60Z40 and A0Z100 suspensions, at a shear rate of 100 s^{-1}.

EPD experiments were performed at 60 °C in the galvanostatic mode applying 0.12 mA cm^{-2} (<0.5 V cm^{-1}) for deposition times up to 10 min, using a power source AMEL, mod. 551 (UK). The configuration of the electrophoresis cell was adapted to coat foil-shaped substrates of graphite as Fig. 1 shows. The graphite electrodes were maintained at a separation distance of 2 cm. The immersion area of the substrates was ∼12.5 cm^2. Withdrawal was performed with a lift at a constant rate of 7.5 mm/s, since this value was found to be suitable in previous work.[26]

Films of each composition were also prepared by dipping graphite substrates on suspensions at 60 °C. Layers were shaped by wetting and gelling at room temperature during the graphite withdrawal.

The kinetics of the continuous and sequential electrophoretic process was also determined for each composition. To determine the continuous kinetics, layers were

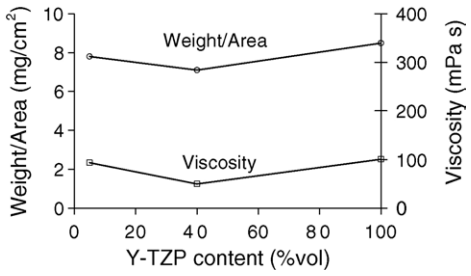

Fig. 3. Relation between the viscosity of the suspensions and the resulting weight per unit area of the dip deposits.

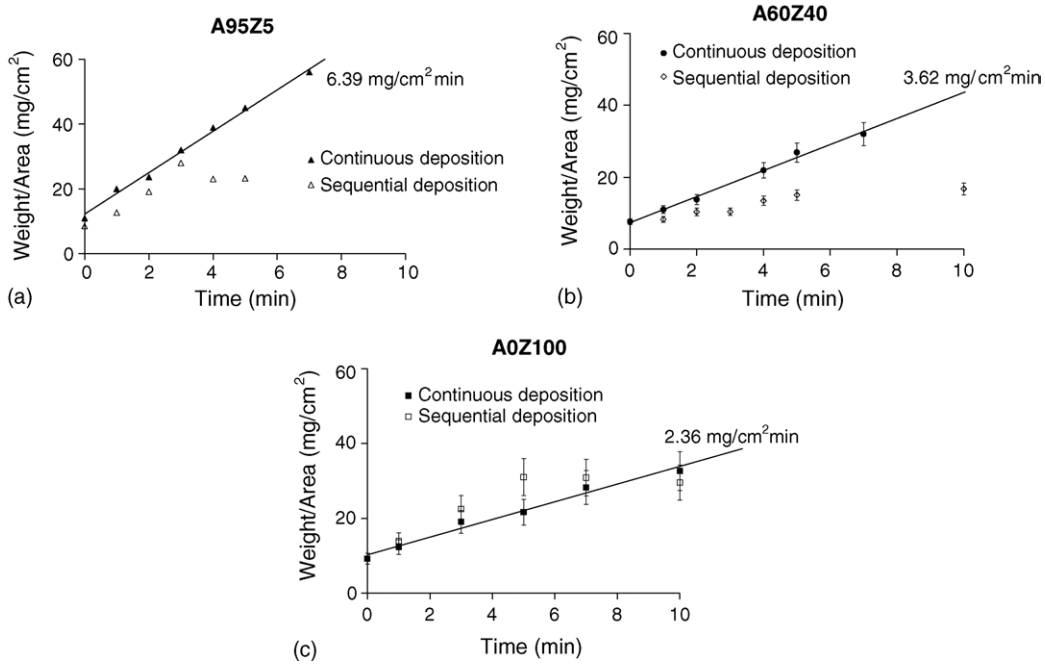

Fig. 4. EPD kinetics of A95Z5, A60Z40 and A0Z100 suspensions (panels a, b, and c, respectively) after continuous and sequential tests.

shaped applying a current density of 0.12 mA cm^{-2} for deposition times up to 10 min. Later, the electrophoretically built layers also gel during withdrawal. The sequential kinetics was determined by performing consecutive EPD tests of 1 min (electrophoresis + gelling) up to 10 times. After the shaping process all deposits were dried at room conditions. The deposited mass was weighted after 24 h drying.

Layered materials were obtained by sequential EPD tests alternating the deposition of slips with different A/Y-TZP ratio. The deposition sequence was: A95Z5, A60Z40, A0Z100, A60Z40 and A95Z5. The deposition time sequences were also controlled in order to obtain layered materials with a symmetrical composition and layers thickness.

Ceramic deposits and substrates were thermally treated at 800 °C for 1 h in air, to remove the graphite, and sintered at 1550 °C for 2 h with heating and cooling rates of 5 °C/min. After sintering, the porosity of self-supported layers was measured by the Archimedes method. Thickness was measured with a digital caliper as the mean value of at least 10 measurements (error, ±10 μm). The theoretical density of the composite materials was calculated by the rule of mixtures, considering the theoretical densities of Al_2O_3 and Y-TZP as 3.97 and 6.1 g cm^{-3}, respectively.

Thickness, microstructures and composition were also studied by Scanning Electron Microscopy and Energy Dispersive X-Ray Spectrometry (SEM-EDX, Zeiss DSM 950, Germany).

The sintered films were diamond machined to obtain samples of 10 mm × 25 mm surface to perform the mechanical tests in a stainless steel three point bending device with 20 mm span. All tests were done in a universal testing machine (Microtest, Spain) using a cross head rate of 0.5 mm/min. The fracture surfaces were observed by SEM to investigate the fracture origins.

Eight samples of each composition were tested to determine the two parameter Weibull distribution of strength. The distribution is given by:[22,27]

$$P_f(\sigma) = 1 - \exp\left(-\frac{\sigma^m}{\sigma_0^m}\right) \quad (1)$$

where $P_f(\sigma)$ is the probability of failure at a stress, σ, σ_0 is a scaling constant and m is the Weibull modulus.

The probability estimator, chosen to give an unbiased estimate of the nth failure when the number of specimens tested is under 20 was:[28,29]

$$P_f = \frac{n - 0.375}{N + 0.25} \quad (2)$$

where N is the total number of specimens tested and n is the specimen rank in ascending order of failure stress.

3. Results and discussion

The evolution of viscosity on cooling at a shear rate of 100 s^{-1} is plotted in Fig. 2. The main properties that control the gelling behaviour of the suspensions (the viscosity at 60 °C, the gelling temperature and the gel strength) are summarized in Table 4. Gelling temperatures are above room temperature (28.4–30 °C) thus allowing the gelation of the layers on withdrawal. Fig. 2 shows that the viscosity of the extreme compositions (A95Z5 and A0Z100), at 60 °C, are in the same range (94 and 101 mPa s, respectively), whereas the intermediate composition (A60Z40) has a lower viscosity

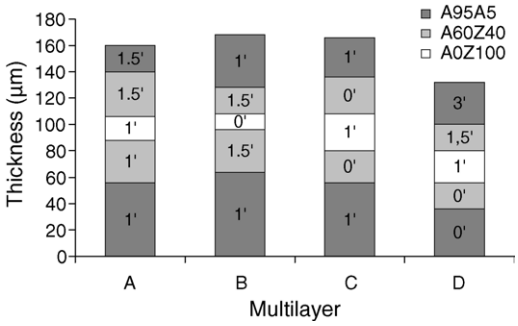

Fig. 5. Thickness of the different layers of laminates obtained at different deposition time sequences.

(50 mPa s). The A60Z40 suspension shows slightly higher gel strength, probably related to a better distribution of polysaccharide as the viscosity of the suspension decreases.

In the dipping process, two homogeneous layers, one on each face of graphite substrate, are formed without any current density applied. Results are expressed for one of these two layers. Fig. 3 plots the weight per unit area of deposits obtained by dipping related to the viscosity at 60 °C (work temperature) of each suspension. The plot demonstrates that the weight of the deposit is directly related to the viscosity of the suspension. The gel strength of the suspensions is high enough to retain the shape of the deposit, just after withdrawal and during drying at room conditions, so that crack-free deposits adhering to the graphite support are obtained.

Electrophoretic deposition kinetics was determined for each composition in order to describe the growth of the layers obtained from optimized suspensions (14 vol.% solids, with 0.6 wt.% of carrageenan). Sequential EPD kinetics of A95Z5, A60Z40 and A0Z100 suspensions are plotted in Fig. 4a–c, and compared to the kinetics obtained in a continuous EPD process for similar deposition times. The plots show the weight values of the deposits obtained from each composition for $t = 0$ (i.e., by dipping). Error bars in Fig. 4b and c indicate the variability of the weight measured for several deposits obtained at similar EPD conditions. The variability of A95Z5 samples is not indicated because it is close to the error of the measurement equipments (around 1–2%). The variability of the deposits weight increased to 10 and 16% for A60Z40 and A0Z100 suspensions, so the process reliability decreases when the Y-TZP concentration increases. Also, the plots of the continuous kinetics show that the deposition rate decreases from 6.39 to 2.36 mg cm^{-2} min^{-1} as the Y-TZP content increases from 5 to 100 vol.%. The introduction of Y-TZP decreases the control of the deposit growth, which changes the deposition rate and the process reliability. SEM studies shows that layers 175 ± 25 μm thick can be obtained after a continuous EPD process for 3, 7 and 10 min with A95Z5, A60Z40 and A0Z100 suspensions, respectively. These conditions were selected to obtain monolithic materials

Table 4
Suspensions properties

Powder composition (vol.%)	Conductivity (mS cm^{-1})	T_g (°C)	η_{60} (mPa s)	η_f/η_i
A95Z5	2.0	30.0	94	>2.7
A60Z40	1.9	28.4	50	>3.1
A0Z100	2.4	30.0	101	>2.7

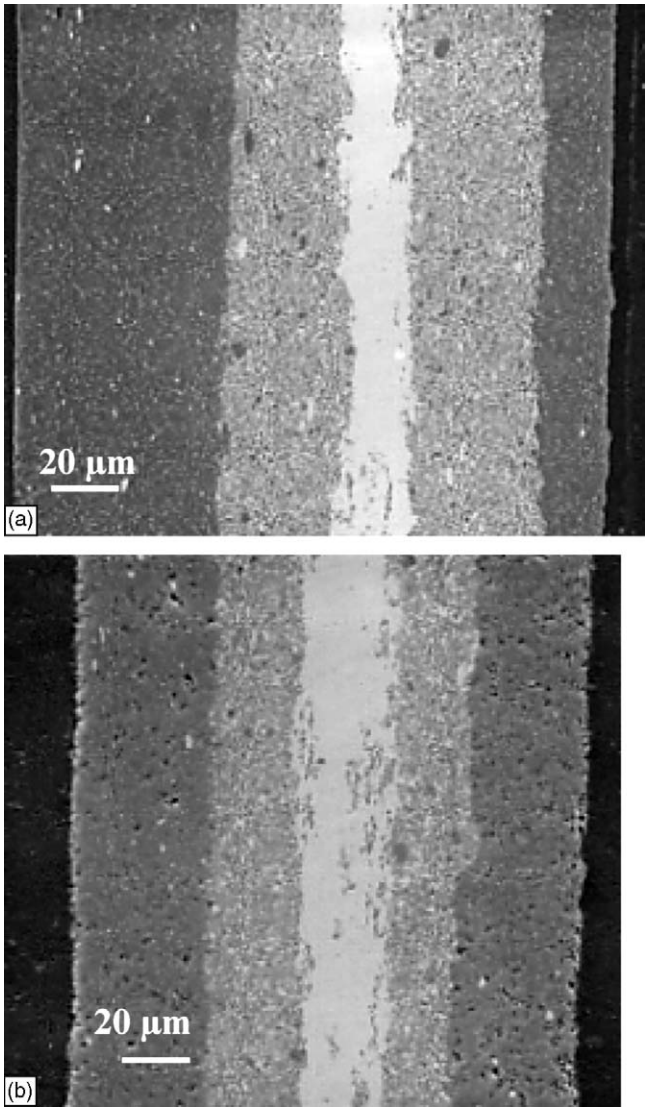

Fig. 6. SEM pictures of laminates A and D of Fig. 5.

Table 5
Strength and Weibull modulus

Material	Thickness (μm)	Weibull modulus (m)	Characteristic strength (σ_0)	Average strength (σ_{50})
A95Z5[a]	172 ± 24	2.9 ± 0.1	180	159
A60Z40	185 ± 41	2.3 ± 0.3	157	135
Z	167 ± 24	5.0 ± 0.5	493	460
Laminate D	193 ± 18	6.7 ± 0.5	181	175

Fitting parameter, $R = 0.97$.
[a] $R = 0.98$

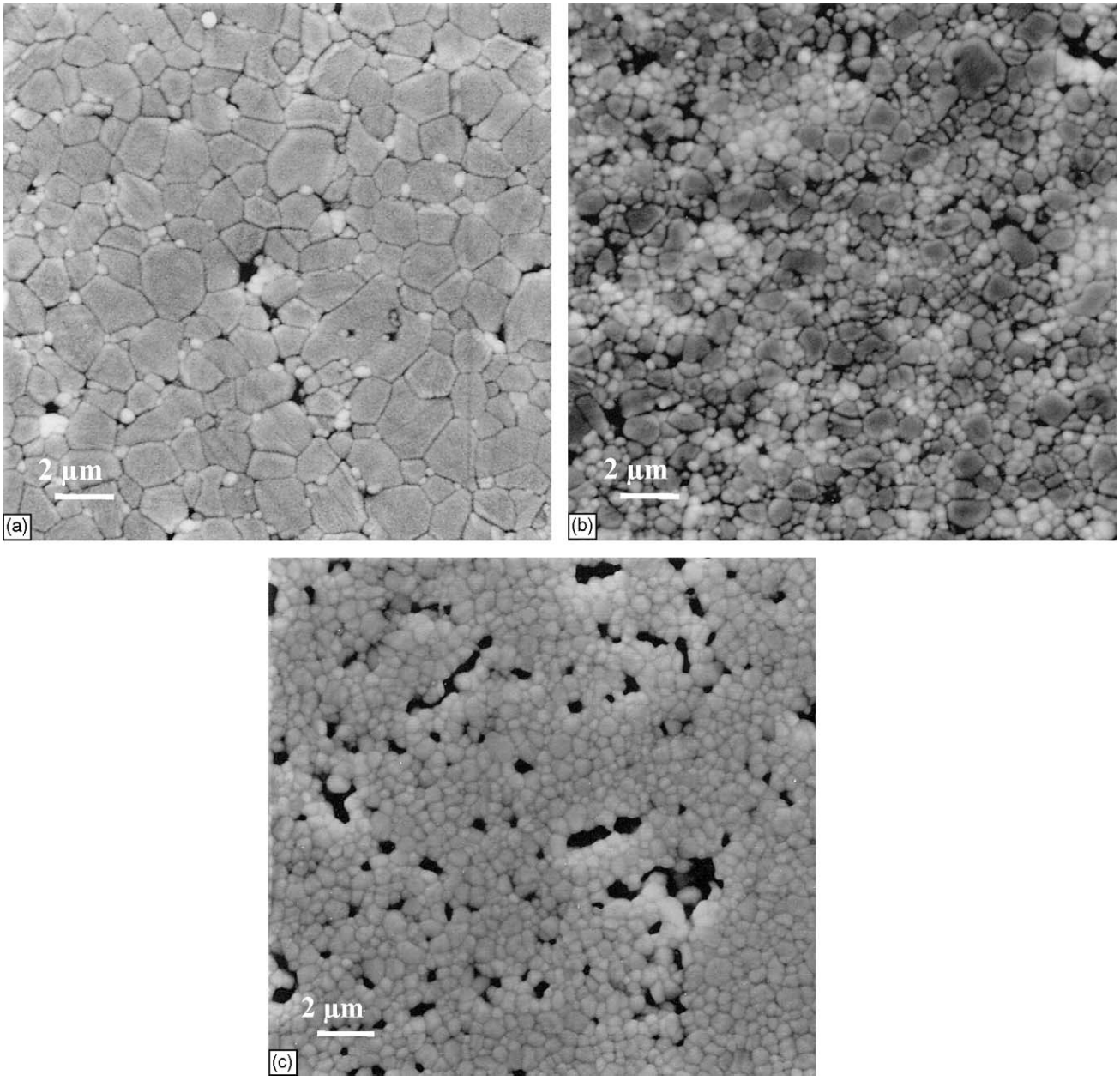

Fig. 7. Characteristic microstructures of monoliths A95Z5 (a), A60Z40 (b) and A0Z100 (c).

of different compositions with similar dimensions, in order to characterize them mechanically.

On the other hand, the sequential deposition has a slower kinetics than that of the continuous process, specially for the A95Z5 composition, becoming rather similar for A0Z100. It would be possible to have a further contribution to the deposit growth after each immersion step and hence, the kinetics would be faster than for the continuous process. The explanation is that in sequential tests the gelled layer is introduced each time in a hot suspension, so that some redissolution of carrageenan at the external surface occurs. As the thickness of the deposit increases this effect becomes more important, thus leading to a plateau in the curves. According to the observed behaviour, it must be expected that the thickness growth of sequential layers will be retarded as the number of layers increases.

Fig. 5 shows several time sequences selected to obtain different layered materials by sequential EPD. Multilayers were characterized by SEM after sintering. The resulting thickness of each layer mainly depends on the deposition time, but also on the cumulative thickness of the previous layers. This effect is clearly seen in material A, where the first layer is thicker than the fifth layer, both having the same composition (A95Z5). In order to obtain a layered material with symmetrical composition and thickness (material D in Fig. 5), times were redesigned taking into account that thickness growth

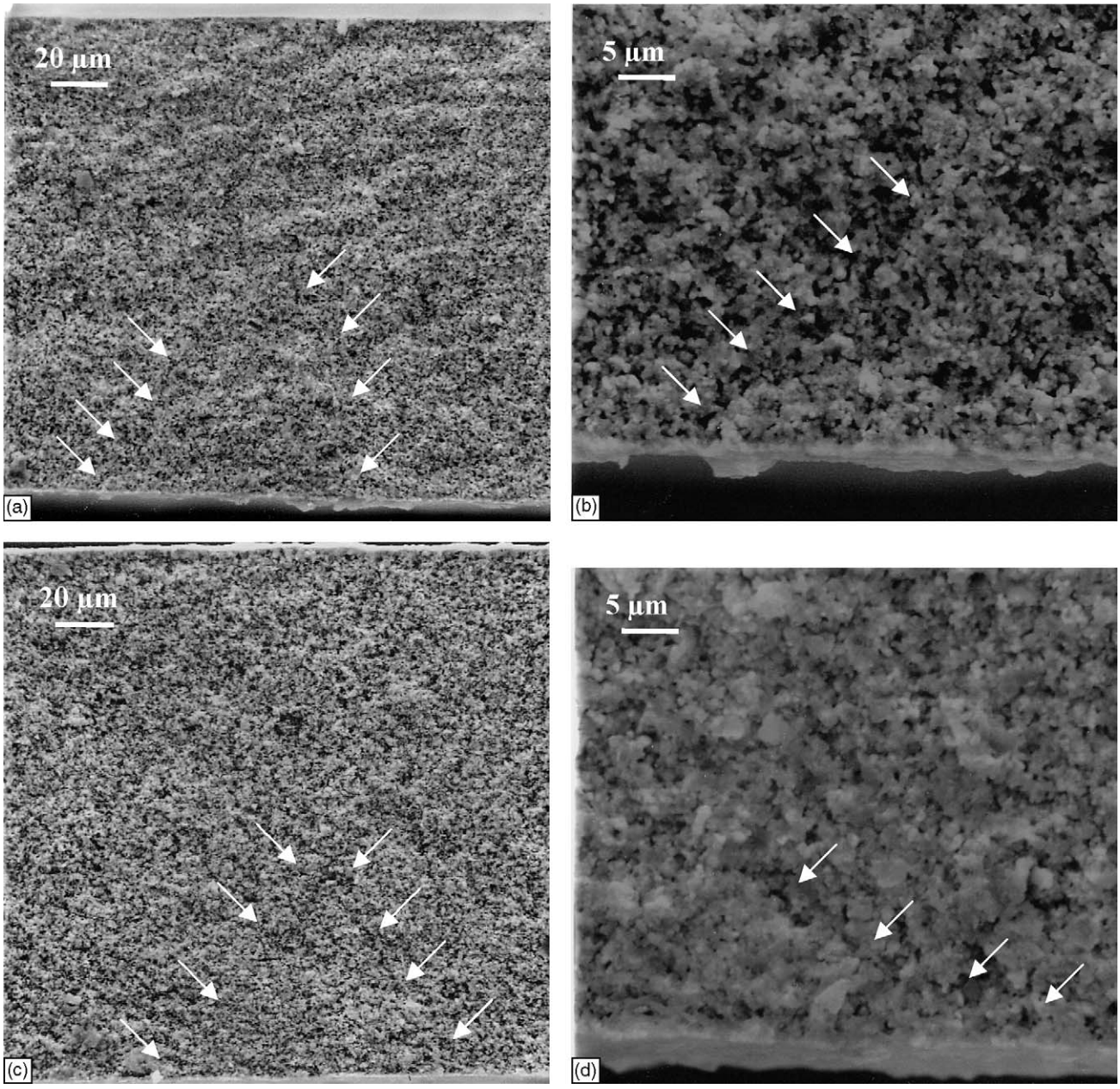

Fig. 8. Pictures at different magnification showing characteristic fracture surfaces of A60Z40 (a and b) and A0Z100 (c and d). Arrows show cracks perpendicular to the fracture surface that propagate towards the middle part of the samples (a and c), from the surface of the specimens (b and d).

decreases with time for all compositions during sequential EPD.

The total thickness of the sintered monoliths is summarized in Table 5 and compared to that of laminate D. Differences between them are inside the variability limits described by the standard deviation, which is larger for the composite A0Z100.

Fig. 6 shows the SEM microstructure of layered materials A and D, respectively. Material D shows much higher symmetry. However, the interfaces are not well defined, especially those in contact with the central layer A0Z100, which occasionally mixes with the adjacent A60Z40 layers. This is also related to a dissolution effect of the carrageenan-containing wet deposit when immersed into the next hot suspension.

SEM observations reveal that the A60Z40 material shows a higher density, although the distribution of the different phases is not as homogeneous as that achieved in materials with a low concentration of second phase (e.g., A95Z5). Fig. 7 shows characteristic microstructures of A60Z40 (Fig. 7b) and A0Z100 (Fig. 7c) compared to that of A95Z5 monolith (Fig. 7a). The strong thermal etching (1450 °C, 1 h) used allows to reveal that the three monoliths have small (<5 μm) elongated pores along the grain boundaries, that sometimes

coalesce to give larger ones, porosity being the highest in A0Z100. The aspect and amount of pores agree with the rather high values of open porosity determined by the Archimedes' method (10–13%) and can be attributed to the effect of gelling agents in the aqueous EPD process.

Fig. 8 shows characteristic fracture surfaces of the monoliths A60Z40 and A0Z100. As in the case of the previously studied A95Z5 plates,[22] at low magnification, it is not possible to discern single critical defects and fracture is very tortuous. There is not a single fracture plane but different flat areas, limited by cracks perpendicular to the fracture surfaces. These cracks start at the surface irregularities and propagate intergranularly, as observed at higher magnification (Figs. 8b,d and 9b). The different flat areas, and the associated cracks, start from the surface in tension during testing and reach different zones of the fracture surfaces, up to the middle part of the samples in some cases (Fig. 8a and c). The same features were observed in the fracture surfaces of the layered plates, in which the flat areas starting from the surface reached half of the thickness of the external A95Z5 layer (Fig. 9a). As occurred in those monoliths, stress concentration at the surface irregularities would originate cracks that easily propagate by linking the elongated pores present in the materials (Fig. 7). Surface irregularities being the fracture origins agreed with the rather low Weibull modulus (Table 5) determined for the previously studied monoliths and with the extremely low and thickness-dependent values of Weibull modulus (0.517–0.682) reported by other authors for thin coatings on stainless steel substrates fabricated by direct-current reactive magneton sputtering.[24]

The Weibull parameters in Eq. (1) were determined from the linear adjustment by the least square method of the plot $\mathrm{Ln}(\mathrm{Ln}(1/(1-P_f)))$ versus $\mathrm{Ln}(\sigma_f)$, as shown in Fig. 10a. Results are summarized in Table 5 and compared with the values corresponding to the monolith studied previously. Even for the small number of samples used, the obtained fits ($R = 0.97$–0.98) are sufficient to establish significant differences between the materials. Considering first the monoliths, strength and Weibull modulus values are the lowest for the monolith A60Z40, even though it should be a tougher and more flaw tolerant material than A95Z5 due to the presence of a significant amount of TZP. These low values should be attributed to the heterogeneous distribution of two phases when both have a similar concentration (Fig. 7b). The linking of the more frequent and larger elongated cracks would lead to the cracks originated at surface irregularities being larger than the maximum size of defect for which the material is flaw tolerant and, therefore, the materials presents low strength and Weibull modulus values.

Strength and Weibull modulus values are larger for material A0Z100 than those corresponding to A95A5 and A60Z40, as expected from the higher toughness and flaw tolerant behaviour of TZP.

The most interesting result is the significant difference between the Weibull modulus of the monolith A95Z5 and that of the laminate with external layers of the same composition.

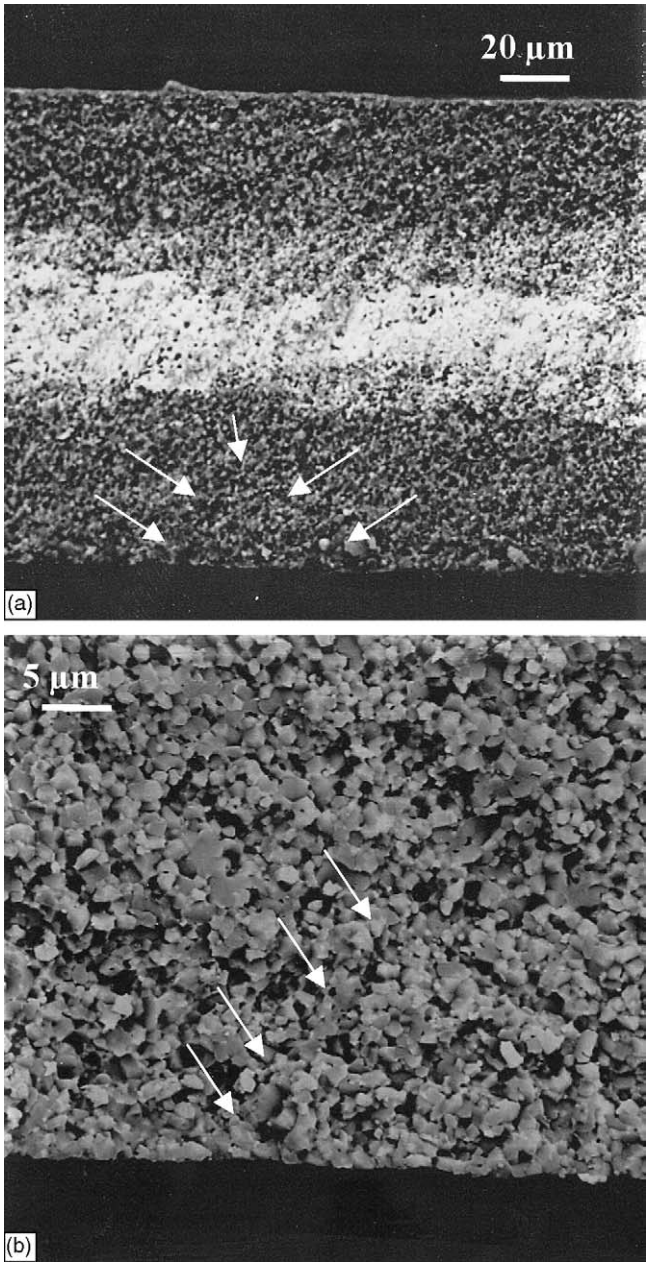

Fig. 9. Characteristic fracture surfaces of the laminate at different magnification. Arrows show cracks perpendicular to the fracture surface, that propagate towards the middle part of the external layer (a) from the surface of the sample (b).

In Fig. 10b the Weibull distributions calculated using the corresponding parameters from Table 5 are plotted for these two materials. The strength values are not significantly higher in the layered material than in the monolith, as shown by the characteristic strength values for probability of failure 63% being similar for both materials, as it could be expected from the possible development of residual stresses due to thermal expansion mismatch of the layers. This fact might be due to the high porosity levels, that would lead to low Young's modulus and, therefore, low values of the residual stresses.

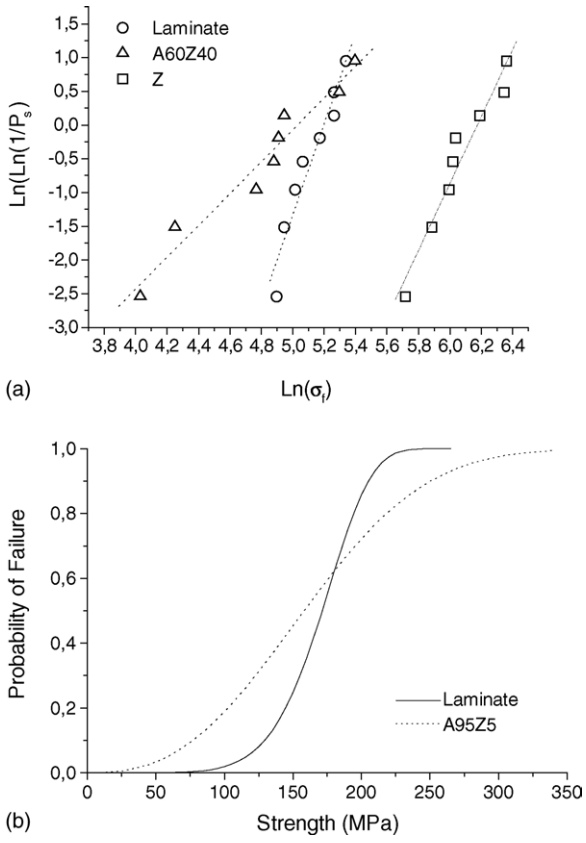

Fig. 10. Weibull analysis of the strength values: (a) $\mathrm{Ln}(\mathrm{Ln}(1/(1-P_f)))$ vs. $\mathrm{Ln}(\sigma_f)$ plot used to determine the Weibull parameters for A60Z40 and A0Z100 monoliths and the laminate; (b) probability of failure of the laminate compared to that of the A95Z5 monolith.

The fact that the strength levels of the laminate are similar to those of the A95Z5 monolith, and significantly lower than those of the monolith of the same composition as the internal A0Z100 layer (Table 5), indicates that the high toughness internal layer has no, or very little, effect on the strength of the laminate.

Conversely, it is apparent the much larger range of failure strengths with non-zero failure probabilities in the monolith, from close to zero strength up to about 350 MPa, as compared to that of the laminate, for which zero probability stands for $\sigma_f \approx 75$ MPa. An interesting feature that has to be pointed out, and systematically studied in other systems, is that limitation of strength values appears to be related mostly from a size effect. Previous work[22] showed that flat cracks starting at the surface of the A95Z5 monolith run up to near half thickness, as it happens in the new compositions studied herein (Fig. 8a and c). The same behaviour is observed here for the laminate (Fig. 9a) but, in this case, the largest surface cracks run just up to the half thickness of the first layer. As discussed above, there are no significant residual stresses in this system and, therefore, it should be concluded that reliability of the laminate, until under critical fracture conditions such as those involved in strength testing, is mostly due to a strong size effect.

4. Conclusions

Self-supported Al_2O_3/Y-TZP multilayers have been manufactured by a gel-deposition process combining either dipping or electrophoretic deposition (EPD) with carrageenan thermogelation. The study of the EPD kinetics of each formulated suspension allows the design of multilayers with controlled thickness in each layer. The three points bending strength values for the laminates are higher than those obtained for a monolithic material with the same composition as that of the external layers. The distribution of the values is well fitted to a simple two parameter Weibull distribution, giving an average modulus of 6.7, which is twice that of the two-phase monolith. Correlation of strength values with fractographic observations demonstrates that the irregularities of the surfaces are the fracture origins in the monoliths, and that the improved reliability of the laminate is mostly due to a strong effect of the reduced thickness of the layers as compared to that of the monolith.

Acknowledgements

This work has been supported by CICYT, Spain (contracts MAT2000-0949 and MAT 2003-836). Work supported in part by the European Community's Human Potential Programme under contract HPRN-CT-2002-00203 [SICMAC]. Dr. Ferrari acknowledges CSIC and European Social Foundation for its financial support.

References

1. Sarkar, P., Haung, X. and Nicholson, P. S., Structural ceramic microlaminate by electrophoretic deposition. *J. Am. Ceram. Soc.*, 1992, **75**(10), 1907–1909.
2. Sarkar, P., Haung, X. and Nicholson, P. S., Electrophoretic deposition and its use to synthesize YSZ/Al_2O_3 microlaminate ceramic/ceramic composites. *Ceram. Eng. Sci. Proc.*, 1993, **14**, 707–716.
3. Bissinger, M., Prakash, O., Sarkar, P. and Nicholson, P. S., High temperatures strength and toughness of electrophoretically deposited alumina/lanthanum aluminate laminates. *Ceram. Eng. Sci. Proc.*, 1994, **15**, 1084–1092.
4. Sarkar, P., Prakash, O., Wang, G. and Nicholson, P. S., Microlaminate ceramic/ceramic composites (YSZ/Al_2O_3) by electrophoretic deposition. *Ceram. Eng. Sci. Proc.*, 1994, **15**, 1019–1027.
5. Fisher, G., Fisher, E., De Portu, G. and Roncari, E., Preparation of ceramic microlaminate by electrophoresis in aqueous system. *J. Mater. Sci. Lett.*, 1995, **14**, 25–27.
6. Vandeperre, L., Van der Biest, O. and Clegg, W. J., Silicon carbide laminates with carbon interlayers by electrophoretic deposition. *Key Eng. Mater.*, 1997, **127–131**, 567–574.
7. Ferrari, B., Sanchez-Herencia, A. J. and Moreno, R., Electrophoretic forming of Al_2O_3/Y-TZP layered ceramics from aqueous suspensions. *Mater. Res. Bull.*, 1998, **33**(3), 487–499.
8. Zhitomirsky, I. and Gal-Or, L., Formation of hollow fibers by electrophoretic deposition. *Mater. Lett.*, 1999, **38**, 10–17.
9. Sarkar, P., Haung, X. and Nicholson, P. S., Zirconia/lumina functionally gradient composites by electrophoretic deposition techniques. *J. Am. Ceram. Soc.*, 1993, **76**, 1055–1056.

10. Ding, X. M., Merk, N. and Ilschner, B., Particle volume graded Ni-Al_2O_3 and Cu-Al_2O_3 composite deposits: production and performances. In *3rd International Symposium on Structural and Functionally Gradient Materials (FGM3), Vol 1*, ed. B. Ilchner and N. Cherradi, 1994, pp. 365–370.
11. Merk, N., Electron microscopy study of the thermal decomposition in Ni-SiC electrodeposits. *J. Mater. Sci. Lett.*, 1995, **14**, 592–595.
12. Barmak, K., Banovic, S. W., Chan, H. M., Friedersdorf, L. E., Harmer, M. P., Marder, A. R. *et al.*, Electrochemical processing of layered composite coatings of nickel-aluminum-alumina/alumina-yttria stabilized zirconia. In *Electrochemical Synthesis and Modification of Materials Symposium*, ed. P. C. Andricacos, S. G. Corcoran, J. L. Delplancke, T. P. Moffat and P. S. Searson. Mater. Res. Soc., Pittsburgh, PA, USA, 1997, pp. 469–474.
13. Sarkar, P., Datta, S. and Nicholson, P. S., Functionally graded ceramic/ceramic and metal/ceramic composites by electrophoretic deposition. In *Composites, Part B (Engineering) (UK), Vol 28B (no 1/2)*. Elsevier, Amsterdam, 1997, pp. 49–56.
14. Zhao, C., Vleugels, J., Vandeperre, L., Basu, B. and Van der Biest, O., Y-TZP/Ce-TZP functionally graded composite. *J. Mater. Sci. Lett.*, 1998, **17**, 1453–1456.
15. Zhao, C., Vleugels, J., Vandeperre, L., Basu, B. and Van der Biest, O., Graded tribological materials formed by electrophoresis. *Mater. Sci. Forum*, 1999, **308–311**, 95–100.
16. Börner, A. and Herbig, R., ESA measurement for electrophoretic deposition of ceramic materials. *Colloid Surf. A: Physicochem. Eng. Aspects*, 1999, **159**, 439–447.
17. Put, S., Anné, G., Vleugels, J. and Van der Biest, O., Functionally graded ZrO_2-WC composites processed by electrophoretic deposition. *Key Eng. Mater.*, 2002, **206–213**, 189–192.
18. Put, S., Vleugels, J. and Van der Biest, O., Functionally graded WC-Co materials produced by electrphoretic deposition. *Scripta Mater.*, 2001, **45**, 1139–1145.
19. Vleugels, J., Anné, G., Put, S. and Van der Biest, O., Thick plate-shape Al_2O_3/ZrO_2 composites with continuous gradient processed by electrophoretic deposition. *Functionally Graded Materials, VII*. Trans. Tech Publications Ltd., Switzerland, 2003, pp. 171–176.
20. Kaya, C., Al_2O_3-Y-TZP/Al_2O_3 functionally graded composites of tubular shape from nano-sols using double-step electrophoretic deposition. *J. Eur. Ceram. Soc.*, 2003, **23**, 1655–1660.
21. Prakash, O., Sarkar, P. and Nicholson, P. S., Crack deflection in ceramic/ceramic laminates with strong interfaces. *J. Am. Ceram. Soc.*, 1995, **78**, 1125–1127.
22. Ferrari, B., González, S., Moreno, R. and Baudín, C., Strength analysis of self-supported films produced by aqueous electrophoretic deposition. *J. Am. Ceram. Soc.* (submitted for publication).
23. Wiklund, U., Hendenqvist, P. and Hogmark, S., Multilayer cracking resistance in bending. *Surf. Coat. Technol.*, 1997, **97**, 773–778.
24. Harry, E., Ignat, M., Pauleau, Y., Rouzaud, A. and Juliet, P., Mechanical behaviour of hard PVD multilayered coatings. *Surf. Coat. Technol.*, 2000, **125**, 185–189.
25. Ferrari, B., Santacruz, I., Nieto, M. I. and Moreno, R., Thermogelation of Al_2O_3/Y-TZP films produced by electrophoretic co-deposition. *J. Eur. Ceram. Soc.*, 2004, **24**, 3073–3080.
26. Santacruz, I., Nieto, M. I., Ferrari, B. and Moreno, R., Ceramic-ceramic laminates by a gel-dipping process. In *Proceedings "Shaping II"*, ed. J. Luyten and J. P. Eraw, 2002, pp. 91–96.
27. Villora, M., Callejas, P., Barba, M. F. and Baudín, C., Statistical analysis of the fracture behaviour of porous ceramic raschig rings. *J. Eur. Ceram. Soc.*, 2004, **24**, 589–594.
28. Bergman, B., On the estimation of the Weibull modulus. *J. Mater. Sci. Lett.*, 1984, **3**, 689–690.
29. Sullivan, J. D. and Lauzon, P. H., Experimental probability estimators for Weibull plots. *J. Mater. Sci. Lett.*, 1986, **5**, 1245–1247.